JOURNAL OF PROPULSION AND POWER
Vol. 23, No. 1, January–February 2007

Acoustic Instability of the Slab Rocket Motor

Sean R. Fischbach,* Joseph Majdalani,† and Gary A. Flandro‡
University of Tennessee Space Institute, Tullahoma, Tennessee 37388

DOI: 10.2514/1.14794

In this article, the evaluation of rotational stability growth rate factors is carried out for the slab rocket motor using a perturbation treatment that is supported by numerical evaluation. The asymptotic expressions for the stability factors are derived over a practical range of operating parameters. For the representative motors under investigation, the analytical estimates are shown to exhibit an error of 5% or less by comparison with numerical integrals. Both numerics and asymptotics converge in predicting less stable systems than projected by irrotational stability theory. The differences can be ascribed to the dismissal of time-dependent rotational coupling in many past studies. The present investigation unravels the details of six additional growth rate corrections. These include the rotational flow, mean vorticity, viscosity, pseudoacoustic, pseudovorticity, and unsteady nozzle growth rate factors. The fourth and fifth terms are due to acoustical and vortical interactions with the often neglected pseudopressure. The sixth is due to the energy associated with the unsteady rotational flow exiting the nozzle. Based on the slab-motor geometry, we find that the flow-turning correction is canceled identically by another rotational term stemming from multidimensional interactions. We also find that the unsteady nozzle damping effect is offset by another source of instability due to the pseudopressure.

Nomenclature

A_p	=	unsteady pressure amplitude
$A_N^{(r)}$	=	nozzle entrance plane admittance
$A_S^{(r)}$	=	inert surface admittance
$A_b^{(r)}$	=	burning surface admittance
a_0	=	mean speed of sound
E	=	time averaged unsteady system energy
E_m^2	=	energy normalization function in mode m, $\frac{5}{4}wl$
$\boldsymbol{e}_y$, $\boldsymbol{e}_z$	=	unit vectors in y and z directions
k_m	=	wave number for axial mode m
L, H	=	chamber length and half-height, $l = L/H$
M_b	=	surface Mach number, V_b/a_0
m	=	oscillation mode shape number
$\boldsymbol{n}$	=	outward pointing unit normal vector
p_0	=	mean pressure
$\boldsymbol{u}$	=	total velocity vector
U_y, U_z	=	mean flow velocities normalized by V_b
W	=	chamber width, $w = W/H$
x	=	action coordinate, $\frac{1}{2}\pi y$
y	=	normal distance from the wall
y, z, t	=	normal, axial, and temporal coordinates
α	=	growth rate (dimensional, $\sec^{-1}$)
δ	=	viscous length, $[\nu/(a_0 H)]^{1/2}$
ε	=	wave amplitude, $A_p/(\gamma p_0)$
γ	=	ratio of specific heats
ρ	=	density
ν	=	kinematic viscosity, μ/ρ
ξ	=	viscous parameter $k_m^2\delta^2/M_b^3$
$\phi(y)$	=	function defined in Eq. (32)
$\psi(y)$	=	exponential argument defined in Eq. (31)
ω, Ω	=	unsteady and mean vorticity magnitudes

Subscripts

b	=	refers to the burning/transpiring surface
i, r	=	irrotational or rotational
m	=	for a given mode number
N, S	=	nozzle or inert surface

Superscripts

$*$	=	dimensional quantity
$\sim$, $\wedge$	=	rotational or acoustical part
r, i	=	part of a complex variable

I. Introduction

THE rising popularity of the slab rocket motor among propulsion analysts may be attributed to the simple geometry that it presents. Clearly, the use of a rectangular-port motor facilitates the design of an experimental setup by incorporating flat segments, screens, and window panels that can drastically improve test calibration and flow visualization capabilities. For the theoretical investigator, it permits the use of Cartesian coordinates which not only reduce the complexity of modeled equations but, also, facilitate the process of constructing the desired solution.

The use of the (opposed plane) slab configuration in combustion stability related studies may be traced back to the work of Brownlee and Marble [1–3] who employed blocks of propellant in some of their laboratory experiments. More recent investigations that adopt the slab geometry include those by Casalis et al. [4–7], Liou et al. [8–10], Yang et al. [11–13], Van Moorhem et al. [14–18], Wasistho et al. at the Center for Simulation of Advanced Rockets (CSAR) [19], and Vuillot et al. at the *Office National d'Études et de Recherches Aérospatiales* (ONERA) [20–25]. In that vein, scientists at both CSAR and ONERA have often utilized the planar/slab configuration as the preferred geometry to either validate their full-scale three-dimensional codes or to concentrate on one particular aspect of motor gas dynamics.

Despite the preponderance of slab-related studies, no fundamental formulation has yet been advanced to assess the acoustic instability

Presented as Paper 4061 at the 40th AIAA/ASME/SAE/ASEE Joint Propulsion Conference and Exhibit, Fort Lauderdale, Florida, 11–14 July 2004; received 23 March 2005; revision received 7 March 2006; accepted for publication 12 March 2006. Copyright © 2006 by Sean R. Fischbach, Joseph Majdalani, and Gary A. Flandro. Published by the American Institute of Aeronautics and Astronautics, Inc., with permission. Copies of this paper may be made for personal or internal use, on condition that the copier pay the $10.00 per-copy fee to the Copyright Clearance Center, Inc., 222 Rosewood Drive, Danvers, MA 01923; include the code $10.00 in correspondence with the CCC.

*Graduate Student and Research Associate, Department of Mechanical, Aerospace and Biomedical Engineering. Member AIAA.

†Jack D. Whitfield Professor of High Speed Flows, Department of Mechanical, Aerospace and Biomedical Engineering, MS-23, 411 B. H. Goethert Parkway, Tullahoma, Tennessee 37388; maji@utsi.edu (corresponding author). Member AIAA.

‡Boling Chair Professor of Excellence in Propulsion, Department of Mechanical, Aerospace and Biomedical Engineering. Associate Fellow AIAA.

characteristics associated with this particular geometry. Past studies have mainly focused on the circular-port configuration as evidenced by the work of Flandro [26–31] and Culick [32–40]. For this reason, it is the purpose of this paper to present the stability correction factors that arise in the two-dimensional motor chamber. This will be accomplished by applying the linear stability formulation introduced by Flandro and Majdalani [27] to the slab configuration. The work will closely follow the steps delineated by Majdalani, Flandro and Fischbach [41] and will briefly compare, in closing, the differences due to the infinite curvature of the slab motor.

II. Geometric Model

The same nomenclature and flow descriptors adopted by Flandro and Majdalani [27] will be used except that a Cartesian coordinate system will be the system of choice. As usual, the chamber will be modeled as a porous rectangular channel with internal half-height/thickness H, width W and overall length L. Assuming that $W \geq 6 \times H$, the passive wall influence is safely ignored [42], and the problem is treated as a case of two-dimensional flow. The flux of gases due to combustion will be modeled by imposing uniform fluid injection along the walls at a constant velocity V_b. Whereas one end of the chamber is closed, the other is open and attached to a choked nozzle. The fluid motion in the chamber is assumed to be symmetric about the midsection plane and laminar. Figure 1 provides sketches of the physical as well as the geometric model.

III. Growth Rate Calculations

Pursuant to established theory [27], the system growth rate for a given oscillation mode can be constructed from the linear superposition of several volume integrals. Using

$$\alpha_m = \alpha_1 + \alpha_2 + \alpha_3 + \cdots = \sum_{i=1}^{N} \alpha_i \tag{1}$$

these integrals can be carried out individually, or in combination, depending on their general form. Naturally, the composite growth rate of the system is a linear sum of these factors. As before, a negative growth rate factor represents an energy sink, while a positive term denotes an instability contributor.

A. First Factor: Extended Pressure Coupling

The first irrotational integrals reported by Flandro and Majdalani [27] are combined to formulate the first correction factor:

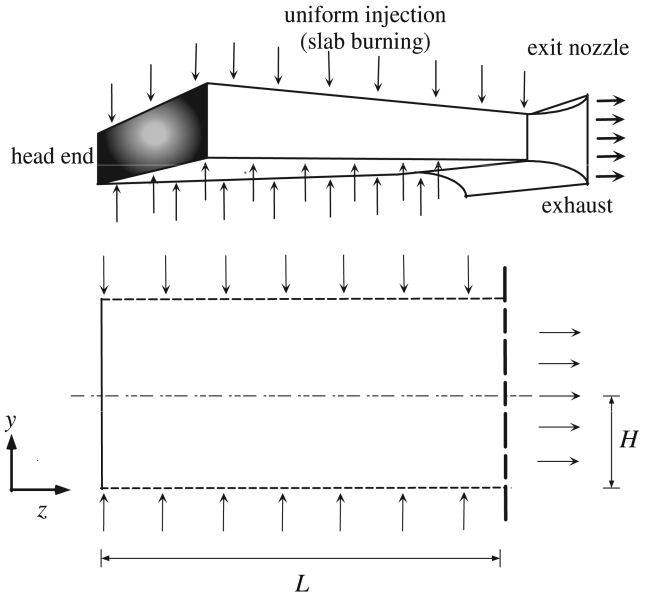

Fig. 1 The geometric model and its coordinate system.

$$\alpha_1 = E_m^{-2} e^{-2\alpha_m t} \iiint_V \Big\langle -\nabla \cdot [\hat{p}\,\hat{\boldsymbol{u}} + \tfrac{1}{2} M_b \boldsymbol{U} (\hat{p})^2] - M_b [\hat{\boldsymbol{u}} \cdot \nabla (\boldsymbol{U} \cdot \hat{\boldsymbol{u}})] \Big\rangle \, \mathrm{d}V \tag{2}$$

Using Gauss's theorem, one transforms the integrand with the divergence operator into a simpler surface integral. One gets

$$\alpha_1 = E_m^{-2} e^{-2\alpha_m t} \left\{ \iint_S \Big\langle \underbrace{-n \cdot [\hat{p}\,\hat{\boldsymbol{u}} + \tfrac{1}{2} M_b \boldsymbol{U} (\hat{p})^2]}_{\mathrm{I}} \Big\rangle \, \mathrm{d}S - \iiint_V \Big\langle \underbrace{M_b [\hat{\boldsymbol{u}} \cdot \nabla (\boldsymbol{U} \cdot \hat{\boldsymbol{u}})]}_{\mathrm{II}} \Big\rangle \, \mathrm{d}V \right\} \tag{3}$$

At this point, vector projections must be carefully evaluated along different sections of the control surfaces delineating the idealized slab-motor chamber. These include, first, along the burning surface,

$$\boldsymbol{n} \cdot \hat{\boldsymbol{u}} = -M_b A_b^{(r)} \hat{p}, \qquad \boldsymbol{n} \cdot \boldsymbol{U} = -1 \tag{4}$$

second, along the inert surface,

$$\boldsymbol{n} \cdot \hat{\boldsymbol{u}} = -M_b A_S^{(r)} \hat{p}, \qquad \boldsymbol{n} \cdot \boldsymbol{U} = 0 \tag{5}$$

and, third, along the nozzle entrance plane,

$$\boldsymbol{n} \cdot \hat{\boldsymbol{u}} = M_b A_N^{(r)} \hat{p}, \qquad \boldsymbol{n} \cdot \boldsymbol{U} = U_N \tag{6}$$

where U_N is the mean axial velocity crossing the nozzle entrance plane at $z = l$.

Knowing that $A_S^{(r)}$ is small compared with other terms, Eqs. (4–6) can be substituted back into Eq. (3). The first integral becomes

$$\mathrm{I} = -E_m^{-2} e^{-2\alpha_m t} M_b \iint_S \Big\langle \hat{p}^2 \Big[-A_b^{(r)} - \tfrac{1}{2} \Big] + \hat{p}^2 \Big[A_N^{(r)} + \tfrac{1}{2} U_N \Big] \Big\rangle \, \mathrm{d}S \tag{7}$$

At this juncture, one may want to insert the value of $\hat{p}^2$ and carry out the time averaging; this operation leads to

$$\mathrm{I} = \tfrac{1}{2} E_m^{-2} M_b \left(\iint_{S_b} \Big\{ \cos^2(k_m z) \Big[A_b^{(r)} + \tfrac{1}{2} \Big] \Big\} \, \mathrm{d}S - \iint_{S_N} \Big\{ \cos^2(k_m z) \Big[A_N^{(r)} + \tfrac{1}{2} U_N \Big] \Big\} \, \mathrm{d}S \right) \tag{8}$$

In much the same way, the second integral of Eq. (3) can be written as

$$\mathrm{II} = -E_m^{-2} e^{-2\alpha_m t} \iiint_V \langle M_b [\hat{\boldsymbol{u}} \cdot \nabla (\boldsymbol{U} \cdot \hat{\boldsymbol{u}})] \rangle \, \mathrm{d}V = E_m^{-2} M_b e^{-2\alpha_m t} \iiint_V \langle (\boldsymbol{U} \cdot \hat{\boldsymbol{u}}) \nabla \cdot \hat{\boldsymbol{u}} \rangle \, \mathrm{d}V \tag{9}$$

where the divergence of the mean flow vector has been set equal to zero. The latter can be expanded into

$$\mathrm{II} = -\tfrac{1}{2} E_m^{-2} M_b e^{-2\alpha_m t} \iiint_V \langle \nabla \cdot (\boldsymbol{U} \hat{p}_m^2) \sin^2(k_m t) \rangle \, \mathrm{d}V \tag{10}$$

Using Gauss's theorem and time averaging, the volumetric integral can be transformed into a surface integral; one obtains

$$\mathrm{II} = -\tfrac{1}{2}M_b E_m^{-2}\iint_S (\tfrac{1}{2}\boldsymbol{n}\cdot\boldsymbol{U}\hat{p}_m^2)\,\mathrm{d}S = \tfrac{1}{2}M_b E_m^{-2}\left(\iint_{S_b}\tfrac{1}{2}\hat{p}_m^2\,\mathrm{d}S - \iint_{S_N}\tfrac{1}{2}U_N\hat{p}_m^2\,\mathrm{d}S\right) \tag{11}$$

Combining Eqs. (8) and (11), Eq. (2) becomes

$$\begin{aligned}\alpha_1 &= \tfrac{1}{2}M_b E_m^{-2}\left\{\iint_{S_b}\tfrac{1}{2}\cos^2(k_m z)\,\mathrm{d}S - \iint_{S_N}[\tfrac{1}{2}U_N\cos^2(k_m z)]\,\mathrm{d}S\right\}\\ &+ \tfrac{1}{2}M_b E_m^{-2}\left(\iint_{S_b}\{\cos^2(k_m z)[A_b^{(r)}+\tfrac{1}{2}]\}\,\mathrm{d}S\right.\\ &\left.+\iint_{S_N}\{\cos^2(k_m z)[-A_N^{(r)}-\tfrac{1}{2}U_N]\}\,\mathrm{d}S\right)\end{aligned} \tag{12}$$

which gives

$$\begin{aligned}\alpha_1 &= \tfrac{1}{2}M_b E_m^{-2}\left\{2\int_0^w\int_0^l \cos^2(k_m z)\left[A_b^{(r)}+1\right]\mathrm{d}z\,\mathrm{d}x\right.\\ &\left.-2\int_0^1\int_0^w \cos^2(k_m z)\left[A_N^{(r)}+U_N\right]\mathrm{d}x\,\mathrm{d}y\right\}\end{aligned} \tag{13}$$

By applying a mass balance to an internal burning slab rocket motor, one gets $2WLV_b = 2WHU_N^*$ or $U_N = l$. Then using $A_N^{(r)} = (\gamma-1)l$, and Eq. (13), the first growth rate factor becomes

$$\alpha_1 = \tfrac{1}{2}lwM_b E_m^{-2}[(A_b^{(r)}+1)-2\gamma] = \tfrac{2}{5}M_b[(A_b^{(r)}+1)-2\gamma] \tag{14}$$

B. Second Factor: Dilatational Energy Correction

The fourth irrotational term leads to

$$\alpha_2 = E_m^{-2}e^{-2\alpha_m t}\iiint_V \langle\tfrac{4}{3}\delta^2\hat{\boldsymbol{u}}\cdot\nabla(\nabla\cdot\hat{\boldsymbol{u}})\rangle\,\mathrm{d}V \tag{15}$$

Using the definition of acoustic velocity and pressure, one can put

$$\begin{aligned}\nabla(\nabla\cdot\hat{\boldsymbol{u}}) &= \nabla[k_m\exp(\alpha_m t)\sin(k_m t)\cos(k_m z)]\\ &= -k_m^2\exp(\alpha_m t)\sin(k_m t)\sin(k_m z)\boldsymbol{e}_z\end{aligned} \tag{16}$$

After time-averaging, Eq. (15) reduces to

$$\alpha_2 = -\tfrac{2}{3}k_m^2\delta^2E_m^{-2}\iiint_V \sin^2(k_m z)\,\mathrm{d}V \tag{17}$$

Using $\mathrm{d}V = \mathrm{d}z\,\mathrm{d}y\,\mathrm{d}x$, the triple integral can be expressed as

$$\begin{aligned}\alpha_2 &= -\tfrac{4}{3}k_m^2\delta^2E_m^{-2}\int_0^w\int_0^1\int_0^l \sin^2(k_m z)\,\mathrm{d}z\,\mathrm{d}y\,\mathrm{d}x = -\tfrac{2}{3}wlk_m^2\delta^2E_m^{-2}\\ &\times[1-\sin(2k_m l)/(2k_m l)] = -\tfrac{2}{3}wlk_m^2\delta^2E_m^{-2} = -\tfrac{8}{15}\xi M_b^3\end{aligned} \tag{18}$$

C. Third Factor: Acoustic Mean Flow Correction

The fifth term can be evaluated from

$$\alpha_3 = E_m^{-2}e^{-2\alpha_m t}\iiint_V \langle M_b\{\hat{\boldsymbol{u}}\cdot(\hat{\boldsymbol{u}}\times\boldsymbol{\Omega})\}\rangle\,\mathrm{d}V \tag{19}$$

Being the mean flow vorticity, $\boldsymbol{\Omega}$ can be approximated from

$$\boldsymbol{\Omega} = \Omega\hat{\boldsymbol{e}}_x = \tfrac{1}{4}\pi^2 z\cos(\theta)\boldsymbol{e}_x \tag{20}$$

and so

$$\hat{\boldsymbol{u}}\times\boldsymbol{\Omega} = \Omega\hat{u}_z\boldsymbol{e}_y - \Omega\hat{u}_y\boldsymbol{e}_z \tag{21}$$

Thus

$$\begin{aligned}\hat{\boldsymbol{u}}\cdot(\hat{\boldsymbol{u}}\times\boldsymbol{\Omega}) &= (\hat{u}_y\boldsymbol{e}_y+\hat{u}_z\boldsymbol{e}_z)\cdot(-\Omega\hat{u}_z\boldsymbol{e}_y+\Omega\hat{u}_y\boldsymbol{e}_z) = -\hat{u}_y\Omega\hat{u}_z\\ &+\hat{u}_z\Omega\hat{u}_y = 0\end{aligned} \tag{22}$$

Evidently, substituting this result into Eq. (19) will cause α_3 to vanish.

D. Fourth Factor: Flow-Turning Correction

The sixth term is a function of the unsteady vorticity. Following standard nomenclature [43], this term will be dubbed "the flow-turning correction." Starting with

$$\begin{aligned}\alpha_4 &= E_m^{-2}e^{-2\alpha_m t}\iiint_V \langle M_b\hat{\boldsymbol{u}}\cdot(\boldsymbol{U}\times\boldsymbol{\omega})\rangle\,\mathrm{d}V\\ &= -E_m^{-2}k_m^{-1}M_b e^{-2\alpha_m t}\iiint_V \langle\nabla\hat{p}\tan(k_m t)\cdot(\boldsymbol{U}\times\boldsymbol{\omega})\rangle\,\mathrm{d}V\end{aligned} \tag{23}$$

one recalls that $\partial\tilde{u}_y/\partial z = \mathcal{O}(M_b^2)$ so that $\boldsymbol{\omega} = \nabla\times\tilde{\boldsymbol{u}} = (\partial\tilde{u}_z/\partial y)\boldsymbol{e}_x$. Using the definition of $\tilde{u}_z$, the unsteady vorticity is expressible by

$$\boldsymbol{\omega} = \exp(\alpha_m t)\left[\frac{\partial\tilde{u}_m^r}{\partial y}\cos(k_m t)+\frac{\partial\tilde{u}_m^i}{\partial y}\sin(k_m t)\right]\boldsymbol{e}_x \tag{24}$$

Then, using the fact that $\boldsymbol{U}\times\boldsymbol{\omega} = (U_z\omega)\boldsymbol{e}_y - (U_y\omega)\boldsymbol{e}_z$, one can rewrite α_4 as

$$\alpha_4 = -E_m^{-2}M_b e^{-2\alpha_m t}\iiint_V \langle\sin(k_m z)e^{\alpha_m t}\sin(k_m t)U_y\omega\rangle\,\mathrm{d}V \tag{25}$$

Equation (25) can be partitioned now into two terms

$$\begin{aligned}\alpha_4 = -\frac{M_b E_m^{-2}}{2e^{2\alpha_m t}}\iiint_V &\underbrace{\left\langle U_y\sin(k_m z)e^{2\alpha_m t}\sin(2k_m t)\frac{\partial\tilde{u}_m^r}{\partial y}\right.}_{\mathrm{I}}\\ &\underbrace{\left.+2U_y\sin(k_m z)e^{2\alpha_m t}\sin^2(k_m t)\frac{\partial\tilde{u}_m^i}{\partial y}\right\rangle}_{\mathrm{II}}\mathrm{d}V\end{aligned} \tag{26}$$

Forthwith, term I gives

$$\begin{aligned}\mathrm{I} &= \left\langle\tfrac{1}{2}U_y\sin(k_m z)\exp(2\alpha_m t)\sin(2k_m t)\frac{\partial\tilde{u}_m^r}{\partial y}\right\rangle\\ &= \frac{k_m}{4\pi}\exp(2\alpha_m t)U_y\sin(k_m z)\frac{\partial\tilde{u}_m^r}{\partial y}\int_0^{2\pi/k_m}\sin(2k_m t)\,\mathrm{d}t = 0\end{aligned} \tag{27}$$

Term II can be calculated from

$$\begin{aligned}\mathrm{II} &= \left\langle U_y\sin(k_m z)e^{2\alpha_m t}\sin^2(k_m t)\frac{\partial\tilde{u}_m^i}{\partial y}\right\rangle\\ &= \tfrac{1}{2}\pi^{-1}k_m e^{2\alpha_m t}U_y\sin(k_m z)\frac{\partial\tilde{u}_m^i}{\partial y}\int_0^{2\pi/k_m}\sin^2(k_m t)\,\mathrm{d}t\\ &= \tfrac{1}{2}e^{2\alpha_m t}U_y\sin(k_m z)\frac{\partial\tilde{u}_m^i}{\partial y}\end{aligned} \tag{28}$$

After combining its separate parts, Eq. (26) reduces to

$$\alpha_4 = -\tfrac{1}{2}M_b E_m^{-2}\iiint_V U_y\sin(k_m z)\frac{\partial\tilde{u}_m^i}{\partial y}\,\mathrm{d}V \tag{29}$$

where the derivative must be evaluated from

$$\frac{\partial\tilde{u}_m^i}{\partial y} = -\cos\eta\exp\phi\frac{\partial(\cos\psi)}{\partial y}\sin(k_m z\cos\eta)+\ldots \tag{30}$$

where

$$\psi(y) = [2k_m/(\pi M_b)]\,\ell_n\left\{\tan\left[\tfrac{1}{4}\pi(1+y)\right]\right\} \tag{31}$$

and

$$\phi(y) = -(\xi/\pi)\left\{\sec(\eta)\tan(\eta) + \ell_n\left\{\tan\left[\tfrac{1}{4}\pi(1+y)\right]\right\}\right\} \tag{32}$$

Only the leading term in this derivative is shown, being one order of magnitude larger than other quantities precipitated from chain-rule differentiation. The latter can be written as

$$\frac{\partial \tilde{u}_m^i}{\partial y} \simeq \frac{k_m}{M_b U_y}\cos(\eta)\exp(\phi)\sin(\psi)\sin[\cos(\eta)k_m z] \tag{33}$$

The first integral with respect to z renders

$$\alpha_4 = -wk_m E_m^{-2}\int_0^1 \cos\left(\tfrac{1}{2}\pi y\right)\left\{-\frac{\sec^2\left(\frac{1}{4}\pi y\right)\sin\left[2k_m l\cos^2\left(\frac{1}{4}\pi y\right)\right]}{4k_m} + \frac{\csc^2\left(\frac{1}{4}\pi y\right)\sin\left[2k_m l\sin^2\left(\frac{1}{4}\pi y\right)\right]}{4k_m}\right\}\sin(\psi)\exp(\phi)\,\mathrm{d}y \tag{34}$$

At this juncture, one must carefully examine the spatial behavior of each term in Eq. (34). One finds that linearization of certain terms will be appropriate prior to integration. To start, both ψ and ϕ must be fully expanded using MacLaurin series; one finds

$$\psi = \left(k_m/M_b\right)\left(y + \tfrac{1}{24}\pi^2 y^3 + \tfrac{1}{384}\pi^4 y^5 + \tfrac{1}{322{,}560}\pi^6 y^7 + \ldots\right) \tag{35}$$

$$\phi = -\xi\left(y + \tfrac{1}{8}\pi^2 y^3 + \tfrac{11}{640}\pi^4 y^5 + \tfrac{241}{107{,}520}\pi^6 y^7 + \ldots\right) \tag{36}$$

It can be easily shown that the leading-order representations for ψ and ϕ yield reasonably accurate approximations. Interestingly, these simple one-term expansions perform fairly adequately, especially near the burning surface where one can put

$$\sin(\psi) = \sin(k_m y/M_b) + \mathcal{O}(y^3) \tag{37}$$

$$\exp(\phi) = \exp(-\xi y) + \mathcal{O}(y^3) \tag{38}$$

To be consistent, all (but the last two terms) remaining in Eq. (34) must be linearized to the order of y^2. The resulting expression for α_4 becomes

$$\alpha_4 = -wk_m E_m^{-2}\int_0^1 \sin(k_m y/M_b)\exp(-\xi y) \times\left[\tfrac{1}{2}l - \tfrac{1}{4}\sin(2k_m l)/k_m\right]\mathrm{d}y \tag{39}$$

At first glance, the exact integral of Eq. (39) appears to be intractable. Nonetheless, an inviscid result can be extracted by suppressing the viscous parameter ξ. The inviscid form of α_4 turns out to be

$$\alpha_4^0 = -\tfrac{1}{2}wlM_b E_m^{-2}[1 - \sin(2k_m l)/(2k_m l)] \tag{40}$$

Knowing that the exact integral must match the inviscid solution in the limit as $\xi \to 0$, we use inductance and reevaluate Eq. (39); at the outset, we find

$$\begin{aligned}\alpha_4 &= -\tfrac{1}{2}wlM_b E_m^{-2}[1 - \sin(2k_m l)/(2k_m l)]\left(1 + M_b^2\xi^2/k_m^2\right)^{-1}\\ &= -\tfrac{1}{2}wlM_b E_m^{-2}\left(1 + M_b^2\xi^2/k_m^2\right)^{-1}\\ &= -\tfrac{2}{5}M_b\left(1 + \pi^{-2}M_b^2\xi^2 l^2 m^{-2}\right)^{-1}\end{aligned} \tag{41}$$

This expression approximates Eq. (23) to within a few percent over a wide range of M_b, ξ, l, and m.

E. Fifth Factor: Rotational Flow Correction

Traditionally only the integrals considered thus far have been accepted in stability assessments. Nevertheless, consistent retention of unsteady rotational terms gives rise to several additional integrals that must not be dismissed. The first rotational flow correction presented by Flandro and Majdalani [27] can be written as

$$\alpha_5 = e^{-2\alpha_m t}E_m^{-2}\iiint_V \langle -\tilde{\boldsymbol{u}}\cdot\nabla\hat{p}\rangle\,\mathrm{d}V \tag{42}$$

The integrand stems from

$$-\tilde{\boldsymbol{u}}\cdot\nabla\hat{p} = k_m\sin(k_m z)\exp(2\alpha_m t)\left[\tilde{u}_m^r\cos^2(k_m t) + \tilde{u}_m^i\sin(k_m t)\cos(k_m t)\right] \tag{43}$$

so that α_5 can be evaluated from

$$\alpha_5 = k_m E_m^{-2}e^{-2\alpha_m t}\iiint_V \langle e^{2\alpha_m t}[\sin(k_m z)\tilde{u}_m^r\cos^2(k_m t) + \sin(k_m z)\tilde{u}_m^i\sin(k_m t)\cos(k_m t)]\rangle\,\mathrm{d}V \tag{44}$$

Carrying out the time-average of the last expression, one gets

$$\alpha_5 = k_m E_m^{-2}\int_0^w \mathrm{d}x\int_0^1\int_0^l \cos(\eta)\exp(\phi)\sin(\psi) \times\sin[k_m z\cos(\eta)]\sin(k_m z)\,\mathrm{d}z\,\mathrm{d}y \tag{45}$$

Following the same lines as before, α_5 becomes

$$\alpha_5 = \tfrac{2}{5}M_b\left(1 + \pi^{-2}M_b^2\xi^2 l^2 m^{-2}\right)^{-1} \tag{46}$$

Except for having an opposite sign, this expression is identical to the flow-turning integral ($\alpha_5 = -\alpha_4$). It demonstrates that, for the slab-motor configuration, the flow-turning term is "exactly canceled" by the rotational flow correction both at leading order and when higher order approximations are retained. This result corresponds to the case for which the simulated burning surface extends over the entire chamber length.

F. Sixth Factor: Mean Vorticity Correction

The fifth rotational term can be written as

$$\alpha_6 = E_m^{-2}e^{-2\alpha_m t}\iiint_V \langle M_b\tilde{\boldsymbol{u}}\cdot(\boldsymbol{U}\times\boldsymbol{\omega})\rangle\,\mathrm{d}V \tag{47}$$

This can be further simplified into

$$\alpha_6 = M_b E_m^{-2}e^{-2\alpha_m t}\iiint_V \langle\exp(\alpha_m t)[\tilde{u}_m^r\cos(k_m t) + \tilde{u}_m^i\sin(k_m t)]\boldsymbol{e}_z \cdot(U_z\omega\boldsymbol{e}_y - U_y\omega\boldsymbol{e}_z)\rangle\,\mathrm{d}V \tag{48}$$

After carrying out the time-averaging operation, one is left with

$$\alpha_6 = -\tfrac{1}{4}M_b E_m^{-2}\iiint_V U_y\left\{\frac{\partial}{\partial y}\left[\left(\tilde{u}_m^r\right)^2 + \left(\tilde{u}_m^i\right)^2\right]\right\}\mathrm{d}V \tag{49}$$

By substituting the values of $\tilde{u}_m^r$ and $\tilde{u}_m^i$ into Eq. (49), one collects

$$\alpha_6 = -\tfrac{1}{4}M_b E_m^{-2}\iiint_V U_y\{\cos^2(\eta)\exp(2\phi)\sin^2[k_m z\cos(\eta)]\}_y\,\mathrm{d}V \tag{50}$$

where the subscript denotes partial differentiation with respect to y. Then, by evaluating

$$\alpha_6 = -\tfrac{1}{4}M_b E_m^{-2} \iiint_V \Big(\{U_y \cos^2(\eta) e^{2\phi} \sin^2[k_m z \cos(\eta)]\}_y - \sin^2[k_m z \cos(\eta)] \cos^2(\eta) e^{2\phi} \frac{\partial}{\partial y} U_y \Big) \, \mathrm{d}V \tag{51}$$

the corresponding triple integral becomes

$$\alpha_6 = \tfrac{1}{2} w M_b E_m^{-2} \int_0^l \sin^2(k_m z) \, \mathrm{d}z - \tfrac{1}{4} w \pi M_b E_m^{-2} \times \int_0^l \int_0^1 \sin^2[k_m z \cos(\eta)] \cos^2(\eta) \sin(\eta) e^{2\phi} \, \mathrm{d}y \, \mathrm{d}z \tag{52}$$

The first integration gives

$$\alpha_6 = \tfrac{1}{4} E_m^{-2} M_b w \Big(l - \pi \int_0^1 \cos^2(\eta) \sin(\eta) e^{2\phi} \tfrac{1}{2} \Big\{ l - \tfrac{1}{2} k_m^{-1} \times \sec\Big(\tfrac{1}{2}\pi y\Big) \sin\Big[2 k_m l \cos\Big(\tfrac{1}{2}\pi y\Big) \Big] \Big\} \, \mathrm{d}y \Big) \tag{53}$$

By asymptotically expanding the latter expression, one arrives at

$$\alpha_6 = \tfrac{1}{4} E_m^{-2} M_b w \Big[l - \pi \int_0^1 e^{2\phi} (\tfrac{1}{4} l \pi y - \tfrac{1}{24} l \pi^3 y^3 + \tfrac{1}{480} l \pi^5 y^5 + \ldots) \, \mathrm{d}y \Big] \tag{54}$$

In the inviscid limit ($\xi = \phi = 0$), Eq. (54) can be evaluated explicitly; based on the form obtained, one may use symbolic programming and the properties of exponentials to estimate the value of the last integral from

$$\alpha_6 = \tfrac{1}{4} E_m^{-2} M_b w \{ l - \tfrac{1}{24} [(k_m \pi \xi^4 e^{2\xi})(\pi^2 - 12)]^{-1} \Big(\tfrac{39}{85} + \tfrac{1}{82}\xi + \tfrac{7}{13} e^{\xi - 107/50} \Big) (4\pi l k_m + 3)(12\xi^2(1 + 2\xi - e^{2\xi}) + \pi^2 \{ 3e^{2\xi} - 3 - 2\xi[3 + \xi(3 + 2\xi)] \}) \} \tag{55}$$

This expression reduces to

$$\alpha_6 = \tfrac{1}{5} M_b \{ 1 - \tfrac{1}{24} [m \pi^2 \xi^4 e^{2\xi} (\pi^2 - 12)]^{-1} \Big(\tfrac{39}{85} + \tfrac{1}{82}\xi + \tfrac{7}{13} e^{\xi - 107/50} \Big) (4m\pi^2 + 3)(12\xi^2(1 + 2\xi - e^{2\xi}) + \pi^2 \{ 3e^{2\xi} - 3 - 2\xi[3 + \xi(3 + 2\xi)] \}) \} \tag{56}$$

G. Seventh Factor: Viscosity Correction

The seventh and eighth rotational groups involve viscous damping expressions. In the classical stability calculations, viscous effects are discounted. A correction to the dilatational effect is represented in the seventh rotational term. Following the same procedure used before, this term can be transformed into a surface integral, viz.

$$\frac{4}{3} \iiint_V \langle \delta^2 \tilde{\boldsymbol{u}} \cdot \nabla (\nabla \cdot \hat{\boldsymbol{u}}) \rangle \, \mathrm{d}V = -\frac{4}{3} \delta^2 \iint_S \langle \boldsymbol{n} \cdot \tilde{\boldsymbol{u}} \partial p^{(1)} / \partial t \rangle \, \mathrm{d}S \tag{57}$$

Clearly, Eq. (57) must be negligible insofar as it scales with the product of δ^2 (see Nomenclature) and the radial unsteady velocity at the boundaries.

The eighth term with viscous damping is not quite negligible. Starting with

$$\alpha_7 = E_m^{-2} e^{-2\alpha_m t} \iiint_V \langle -\delta^2 (\hat{\boldsymbol{u}} + \tilde{\boldsymbol{u}}) \cdot (\nabla \times \boldsymbol{\omega}) \rangle \, \mathrm{d}V \tag{58}$$

one may set

$$\alpha_7 = \delta^2 E_m^{-2} \exp(-2\alpha_m t) \iiint_V \langle A + B \rangle \, \mathrm{d}V \tag{59}$$

where $A = -\hat{\boldsymbol{u}} \cdot (\nabla \times \boldsymbol{\omega})$ and $B = -\tilde{\boldsymbol{u}} \cdot (\nabla \times \boldsymbol{\omega})$ so that

$$A = -\hat{\boldsymbol{u}} \cdot (\nabla \times \boldsymbol{\omega}) = e^{\alpha_m t} \sin(k_m z) \sin(k_m t) \frac{\partial^2 \tilde{u}}{\partial y^2} \tag{60}$$

$$B = -\tilde{\boldsymbol{u}} \cdot (\nabla \times \boldsymbol{\omega}) = e^{\alpha_m t} \Big[\tilde{u}_m^r \cos(k_m t) + \tilde{u}_m^i \sin(k_m t) \Big] \frac{\partial^2 \tilde{u}}{\partial y^2} \tag{61}$$

Using standard descriptors, the second derivative can be partitioned into

$$\frac{\partial^2 \tilde{u}}{\partial y^2} = \exp(\alpha_m t) \left[\frac{\partial^2 \tilde{u}_m^r}{\partial y^2} \cos(k_m t) + \frac{\partial^2 \tilde{u}_m^i}{\partial y^2} \sin(k_m t) \right] \tag{62}$$

Substituting back into A and B, one gathers

$$A = \sin(k_m z) \exp(2\alpha_m t) \left[\frac{\partial^2 \tilde{u}_m^r}{\partial y^2} \sin(k_m t) \cos(k_m t) + \frac{\partial^2 \tilde{u}_m^i}{\partial y^2} \sin^2(k_m t) \right] \tag{63}$$

and

$$B = \exp(2\alpha_m t) \left[\tilde{u}_m^r \frac{\partial^2 \tilde{u}_m^r}{\partial y^2} \cos^2(k_m t) + \tilde{u}_m^i \frac{\partial^2 \tilde{u}_m^i}{\partial y^2} \sin^2(k_m t) + \tilde{u}_m^r \frac{\partial^2 \tilde{u}_m^i}{\partial y^2} \cos(k_m t) \sin(k_m t) + \tilde{u}_m^i \frac{\partial^2 \tilde{u}_m^r}{\partial y^2} \cos(k_m t) \sin(k_m t) \right] \tag{64}$$

After insertion into Eq. (59), time-averaging enables us to reduce these expressions into

$$\alpha_7 = \frac{1}{2} \frac{\delta^2}{E_m^2} \iiint_V \left[\tilde{u}_m^r \frac{\partial^2 \tilde{u}_m^r}{\partial y^2} + \tilde{u}_m^i \frac{\partial^2 \tilde{u}_m^i}{\partial y^2} + \sin(k_m z) \frac{\partial^2 \tilde{u}_m^i}{\partial y^2} \right] \mathrm{d}V \tag{65}$$

Using the same asymptotic rationale for expanding Eq. (33), on can put

$$\frac{\partial^2 \tilde{u}_m^i}{\partial y^2} \simeq \left(\frac{k_m}{M_b U_y} \right)^2 \cos(\eta) \exp(\phi) \cos(\psi) \sin[\cos(\eta) k_m z] \tag{66}$$

and

$$\frac{\partial^2 \tilde{u}_m^r}{\partial y^2} \simeq -\left(\frac{k_m}{M_b U_y} \right)^2 \cos(\eta) \exp(\phi) \sin(\psi) \sin[\cos(\eta) k_m z] \tag{67}$$

The integral becomes

$$\alpha_7 = \tfrac{1}{2} E_m^{-2} \delta^2 k_m^2 M_b^{-2} \iiint_V \{ \sec(\eta) e^{\phi} \cos(\psi) \sin(k_m z) \sin[k_m z \cos(\eta)] - e^{2\phi} \sin^2[k_m z \cos(\eta)] \} \, \mathrm{d}V \tag{68}$$

Asymptotically, it can be shown that

$$|\sec(\eta) \exp(\phi) \cos(\psi) \sin(k_m z) \sin[k_m z \cos(\eta)]| \ll |\exp(2\phi) \sin^2[k_m z \cos(\eta)]| \tag{69}$$

Therefore, this integral collapses into

$$\alpha_7 = -\tfrac{1}{2} E_m^{-2} \delta^2 k_m^2 M_b^{-2} \iiint_V \exp(2\phi) \sin^2[k_m z \cos(\eta)] \, \mathrm{d}V \tag{70}$$

As usual, expanding the triple integral renders

$$\alpha_7 = -E_m^{-2}\delta^2 k_m^2 M_b^{-2}\int_0^w\int_0^l\int_0^1 \{\exp(2\phi)\sin^2[k_m z\sin(\eta)]\}\,\mathrm{d}y\,\mathrm{d}z\,\mathrm{d}x \tag{71}$$

so that

$$\alpha_7 = -\tfrac{1}{2}wE_m^{-2}\delta^2 k_m^2 M_b^{-2}\int_0^1 \exp(2\phi)\{l-\tfrac{1}{2}k_m^{-1} \times \sec(\eta)\sin[2k_m l\cos(\eta)]\}\,\mathrm{d}y \tag{72}$$

Recalling Eq. (36), subsequent linearization and integration lead to

$$\alpha_7 = -\tfrac{1}{8}(24lk_m-\pi^3)^{-1}wE_m^{-2}\delta^2\xi^{-3}k_m M_b^{-2}\left(\tfrac{21}{32}+\tfrac{19}{56}e^{\xi-27/10}\right)(lk_m - \tfrac{11}{91}\pi)(3e^{-2\xi}\{16lk_m\xi^2(e^{2\xi}-1)+\pi^3[1-e^{2\xi}+2\xi(1+\xi)]\}) \tag{73}$$

or, written differently,

$$\alpha_7 = -\tfrac{1}{10}\pi^2(24m-\pi^2)^{-1}m(m-\tfrac{11}{91})l^{-2}\delta^2\xi^{-3}M_b^{-2}\left(\tfrac{21}{32} + \tfrac{19}{56}e^{\xi-27/10}\right)(3e^{-2\xi}\{16m\xi^2(e^{2\xi}-1)+\pi^2[1-e^{2\xi}+2\xi(1 + \xi)]\}) \tag{74}$$

H. Eighth Factor: Pseudo Acoustic Correction

The last two terms are due to the coupling between the pseudopressure associated with the vortical field and either the unsteady acoustical or rotational velocities. The first term can be expressed by

$$\alpha_8 = E_m^{-2}e^{-2\alpha_m t}\iiint_V \langle -\hat{\boldsymbol{u}}\cdot\nabla\tilde{p}\rangle\,\mathrm{d}V \tag{75}$$

Following the usual form [27], one writes

$$\tilde{p} = \exp(\alpha_m t)\left[\tilde{p}_m^r\cos(k_m t)+\tilde{p}_m^i\sin(k_m t)\right] \tag{76}$$

where

$$\tilde{p}_m^r = -\tfrac{1}{2}\pi M_b z\sin(\psi)\sin(\eta)\cos(\eta)\exp(\phi)\sin[k_m z\cos(\eta)] \tag{77}$$

and

$$\tilde{p}_m^i = \tfrac{1}{2}\pi M_b z\cos(\psi)\sin(\eta)\cos(\eta)\exp(\phi)\sin[k_m z\cos(\eta)] \tag{78}$$

Accordingly,

$$\nabla\tilde{p} = \exp(\alpha_m t)\left[\cos(k_m t)\nabla\tilde{p}_m^r+\sin(k_m t)\nabla\tilde{p}_m^i\right] \tag{79}$$

where

$$\nabla\tilde{p}_m^r = \frac{\partial}{\partial y}\left(\tilde{p}_m^r\right)\boldsymbol{e}_y+\frac{\partial}{\partial z}\left(\tilde{p}_m^r\right)\boldsymbol{e}_z \simeq -\tfrac{1}{2}\pi(k_m/U_y)z\cos(\psi)\sin(\eta) \times\cos(\eta)\exp(\phi)\sin[k_m z\cos(\eta)]\boldsymbol{e}_y-\tfrac{1}{2}\pi M_b\sin(\psi)\sin(\eta) \times\cos(\eta)\exp(\phi)\{\sin[k_m z\cos(\eta)]+k_m z\cos(\eta) \times\cos[k_m z\cos(\eta)]\}\boldsymbol{e}_z \tag{80}$$

and

$$\nabla\tilde{p}_m^i = \frac{\partial}{\partial y}(\tilde{p}_m^i)\boldsymbol{e}_r+\frac{\partial}{\partial z}(\tilde{p}_m^i)\boldsymbol{e}_z \simeq -\tfrac{1}{2}\pi(k_m/U_y)z\sin(\psi)\sin(\eta) \times\cos(\eta)\exp(\phi)\sin[k_m z\cos(\eta)]\boldsymbol{e}_y+\tfrac{1}{2}\pi M_b\cos(\psi)\sin(\eta) \times\cos(\eta)\exp(\phi)\{\sin[k_m z\cos(\eta)]+k_m z\cos(\eta) \times\cos[k_m z\cos(\eta)]\}\boldsymbol{e}_z \tag{81}$$

Before time averaging, the integrand in α_8 can be expanded into

$$\hat{\boldsymbol{u}}\cdot\nabla\tilde{p} \simeq \tfrac{1}{2}\pi M_b\exp(2\alpha_m t)\sin(k_m z)\sin(k_m t)\sin(\eta) \times\cos(\eta)\exp(\phi)\{\sin[k_m z\cos(\eta)]+k_m z\cos(\eta) \times\cos[k_m z\cos(\eta)]\}[\cos(\psi)\sin(k_m t)-\sin(\psi)\cos(k_m t)] \tag{82}$$

hence,

$$\langle\hat{\boldsymbol{u}}\cdot\nabla\tilde{p}\rangle = \tfrac{1}{4}\pi M_b e^{2\alpha_m t}\sin(k_m z)\sin(\eta)\cos(\eta)e^{\phi}\cos(\psi)\{\sin \times[k_m z\cos(\eta)]+k_m z\cos(\eta)\cos[k_m z\cos(\eta)]\} \tag{83}$$

The corresponding integral becomes

$$\alpha_8 = -\tfrac{1}{4}\pi M_b E_m^{-2}\iiint_V \exp(\phi)\sin(k_m z)\sin(\eta)\cos(\eta)\cos(\psi) \times\{\sin[k_m z\cos(\eta)]+k_m z\cos(\eta)\cos[k_m z\cos(\eta)]\}\,\mathrm{d}V \tag{84}$$

This can be evaluated from

$$\alpha_8 = -\tfrac{1}{2}\pi M_b E_m^{-2}\int_0^w\int_0^l\int_0^1 \sin(k_m z)\sin(\eta)\cos(\eta)e^{\phi}\cos(\psi) \times\{\sin[k_m z\cos(\eta)]+k_m z\cos(\eta)\cos[k_m z\cos(\eta)]\}\,\mathrm{d}y\,\mathrm{d}z\,\mathrm{d}x = -\tfrac{1}{2}\pi wM_b E_m^{-2}\int_0^l\int_0^1 \sin(k_m z)\sin(\eta)\cos(\eta)e^{\phi}\cos(\psi) \times\{\sin[k_m z\cos(\eta)]+k_m z\cos(\eta)\cos[k_m z\cos(\eta)]\}\,\mathrm{d}y\,\mathrm{d}z \tag{85}$$

At this juncture, one can directly integrate Eq. (85) with respect to z. The outcome is

$$\alpha_8 = -\tfrac{1}{2}\pi wM_b E_m^{-2}\int_0^1 Q(y)\,\mathrm{d}y \tag{86}$$

where

$$Q(y) = \frac{1}{64k_m}\exp(\phi)\cos(\psi)\sin(\eta)\cos(\eta)(\{lk_m\cos(\eta) \times\cos[k_m l\cos(\eta)]\csc^4(\tfrac{1}{4}\pi y)\sec^4(\tfrac{1}{4}\pi y)[\cos(lk_m-\pi y) + \cos(lk_m+\pi y)-2\cos(lk_m)]\}+\tfrac{1}{4}\{\csc^4(\tfrac{1}{4}\pi y)\sec^4(\tfrac{1}{4}\pi y) \times[lk_m\sin(lk_m-2\pi y)+lk_m\sin(lk_m+2\pi y)-24\cos(lk_m) - 4\cos(lk_m-\pi y)-4\cos(lk_m+\pi y)]\sin[k_m l\cos(\eta)]\}) \tag{87}$$

The result must then be linearized and integrated with respect to y. One obtains

$$\alpha_8 \simeq -\tfrac{1}{2}w\pi M_b E_m^{-2}\int_0^1 e^{-\xi y}\cos(k_m y/M_b)\left\{\tfrac{1}{8}l\pi y+y^3\left[-\tfrac{1}{48}l\pi^3 + \tfrac{1}{2}\pi\left(\tfrac{1}{60}l\pi^2-\tfrac{1}{96}\pi^2 l^3 k_m^2+\ldots\right)\right]\right\}\mathrm{d}y \tag{88}$$

and so

$$\alpha_8 = -\tfrac{1}{16}w\pi^2 lM_b^3 E_m^{-2}\left(\xi^2M_b^2-k_m^2\right)\left(\xi^2M_b^2+k_m^2\right)^{-2} \tag{89}$$

This can be rearranged into

$$\alpha_8 = -\tfrac{1}{20}\pi^2 M_b^3\left(\xi^2M_b^2-m^2\pi^2l^{-2}\right)\left(\xi^2M_b^2+m^2\pi^2l^{-2}\right)^{-2} \tag{90}$$

I. Ninth Factor: Pseudo Vorticity Correction

The last term is due to the less obvious coupling that is formed between vorticity-induced pseudopressure and the unsteady rotational velocity. The significance of this term can be derived from

$$\alpha_9 = -E_m^{-2} e^{-2\alpha_m t} \iiint_V \langle \tilde{\boldsymbol{u}} \cdot \nabla \tilde{p} \rangle \, \mathrm{d}V \tag{91}$$

One carries out the time averaging to obtain

$$\begin{aligned}\langle \tilde{\boldsymbol{u}} \cdot \nabla \tilde{p} \rangle = {} & -\tfrac{1}{4}\pi M_b \exp(2\alpha_m t) \exp(2\phi) \cos^2(\eta) \sin(\eta) \\ & \times \sin^2[k_m z \cos(\eta)] (k_m z \cos(\eta) \cot[k_m z \cos(\eta)] \\ & + \{1 + z k_m \cos(\eta) \cot[k_m z \cos(\eta)]\})\end{aligned} \tag{92}$$

The volumetric integral becomes

$$\begin{aligned}\alpha_9 = {} & \tfrac{1}{4}\pi M_b E_m^{-2} \iiint_V \exp(2\phi) \cos^2(\eta) \sin(\eta) \sin^2[k_m z \cos(\eta)] \\ & \times (k_m z \cos(\eta) \cot[k_m z \cos(\eta)] + \{1 + z k_m \cos(\eta) \\ & \times \cot[k_m z \cos(\eta)]\}) \, \mathrm{d}V\end{aligned} \tag{93}$$

and so,

$$\begin{aligned}\alpha_9 = {} & \tfrac{1}{2}\pi w M_b E_m^{-2} \int_0^l \int_0^1 \exp(2\phi) \cos^2(\eta) \sin(\eta) \sin^2[k_m z \cos(\eta)] \\ & \times (k_m z \cos(\eta) \cot[k_m z \cos(\eta)] + \{1 + z k_m \cos(\eta) \\ & \times \cot[k_m z \cos(\eta)]\}) \, \mathrm{d}y \, \mathrm{d}z\end{aligned} \tag{94}$$

Next, the integral with respect to z is evaluated. The subsequent expression is transformed into y, linearized near the wall, and integrated term-by-term. After some effort, one finds

$$\alpha_9 = \tfrac{1}{2}\pi w l M_b E_m^{-2} \int_0^1 \exp(2\phi) \cos^2(\eta) \sin(\eta) \sin^2[k_m z \cos(\eta)] \, \mathrm{d}y \tag{95}$$

Equation (95) requires an asymptotic treatment that relies, in part, on trigonometric identities. One collects

$$\alpha_9 = \tfrac{1}{2}\pi w l M_b E_m^{-2} \int_0^1 (\tfrac{1}{2}\pi y - \tfrac{7}{48}\pi^3 y^3 + \tfrac{61}{3840}\pi^5 y^5 + \ldots) \, \mathrm{d}y \tag{96}$$

which, at length, gives

$$\begin{aligned}\alpha_9 = {} & \tfrac{1}{6} w l M_b E_m^{-2} \left(1 - \tfrac{3}{2}\pi^{-2}\right) \left(\tfrac{427}{425} + \tfrac{917}{374}\xi + \tfrac{95}{61}\xi^2 + \tfrac{437}{670}\xi^3 \right. \\ & \left. + \tfrac{101}{847}\xi^4 + \tfrac{1}{65}\xi^5 + \tfrac{1}{794}\xi^6\right)^{-1}\end{aligned} \tag{97}$$

otherwise, one can put

$$\begin{aligned}\alpha_9 = {} & \tfrac{2}{15} M_b \left(1 - \tfrac{3}{2}\pi^{-2}\right) \left(\tfrac{427}{425} + \tfrac{917}{374}\xi + \tfrac{95}{61}\xi^2 + \tfrac{437}{670}\xi^3 + \tfrac{101}{847}\xi^4 \right. \\ & \left. + \tfrac{1}{65}\xi^5 + \tfrac{1}{794}\xi^6\right)^{-1}\end{aligned} \tag{98}$$

J. Tenth Factor: Unsteady Nozzle Correction

The tenth correction factor in stability calculations is due to the unsteady rotational energy crossing the motor exit plane. This growth rate is precipitated by the third and fourth rotational terms; these can be lumped together into

$$\alpha_{10} = -M_b E_m^{-2} e^{-2\alpha_m t} \iiint_V \langle (\hat{\boldsymbol{u}} + \tilde{\boldsymbol{u}}) \cdot \nabla (\boldsymbol{U} \cdot \tilde{\boldsymbol{u}}) \rangle \, \mathrm{d}V \tag{99}$$

This triple integral can be converted using

$$\begin{aligned}\alpha_{10} = {} & -M_b E_m^{-2} e^{-2\alpha_m t} \iint_{S_N} \langle [\boldsymbol{n} \cdot (\hat{\boldsymbol{u}} + \tilde{\boldsymbol{u}})] (\boldsymbol{U} \cdot \tilde{\boldsymbol{u}}) \rangle \, \mathrm{d}S \\ = {} & -M_b E_m^{-2} e^{-2\alpha_m t} \iint_{S_N} \left\langle \tilde{u}_z^2 U_z \right\rangle \mathrm{d}S + \mathcal{O}\left(M_b^2\right)\end{aligned} \tag{100}$$

one gets

$$\begin{aligned}\alpha_{10} = {} & -\tfrac{1}{2}\pi M_b E_m^{-2} e^{-2\alpha_m t} \iint_{S_N} \langle z \cos^2(\eta) \sin^2[k_m z \cos(\eta)] \\ & \times e^{2\phi} e^{2\alpha_m t} [\cos^2(\psi) \sin^2(k_m t) + \sin^2(\psi) \cos^2(k_m t) \\ & - 2 \cos(\psi) \sin(k_m t) \sin(\psi) \cos(k_m t)] \sin(\eta) \rangle \, \mathrm{d}S\end{aligned} \tag{101}$$

which, after time-averaging, yields

$$\alpha_{10} = -\tfrac{1}{4}\pi M_b E_m^{-2} \iint_{S_N} z \exp(2\phi) \cos^2(\eta) \sin(\eta) \sin^2[k_m z \cos(\eta)] \, \mathrm{d}S \tag{102}$$

and so

$$\begin{aligned}\alpha_{10} = {} & -\tfrac{1}{2}\pi l M_b E_m^{-2} \int_0^w \int_0^1 \exp(2\phi) \cos^2(\eta) \\ & \times \sin(\eta) \sin^2[k_m z \cos(\eta)] \, \mathrm{d}y \, \mathrm{d}x\end{aligned} \tag{103}$$

Subsequent integration gives

$$\alpha_{10} = -\tfrac{1}{2}\pi w l M_b E_m^{-2} \int_0^1 \exp(2\phi) \cos^2(\eta) \sin(\eta) \sin^2[k_m z \cos(\eta)] \, \mathrm{d}y \tag{104}$$

which can be expressed as

$$\begin{aligned}\alpha_{10} = {} & -\frac{4}{27} M_b \left(1 - \tfrac{3}{2}\pi^{-2}\right) \left(\tfrac{427}{425} + \tfrac{917}{374}\xi + \tfrac{95}{61}\xi^2 + \tfrac{437}{670}\xi^3 + \tfrac{101}{847}\xi^4 \right. \\ & \left. + \tfrac{1}{65}\xi^5 + \tfrac{1}{794}\xi^6\right)^{-1}\end{aligned} \tag{105}$$

Remarking that $\alpha_{10} = -\alpha_9$, the last two factors cancel out identically.

IV. Discussion

A. Standard Formulation

The degree of refinement associated with the current results may be assessed by comparing the rotational predictions with those derived from the irrotational stability formulation. Again, the characteristic parameters of the four representative cases introduced by Flandro [43] will be used. As indicated earlier, the classical stability formulation does not retain unsteady rotational effects except through the flow-turning term, which is indeed needed in a one-dimensional representation. In essence, the growth rate predicted by the irrotational model consists of

$$\begin{aligned}\alpha_i = \alpha_{1\text{–}4} = {} & -\tfrac{1}{2} w l M_b E_m^{-2} \gamma_b - \tfrac{2}{3} w l k_m^2 \delta^2 E_m^{-2} - \tfrac{1}{2} w l M_b E_m^{-2} \\ & \times \left(1 + M_b^2 \xi^2 / k_m^2\right)^{-1}\end{aligned} \tag{106}$$

where $\gamma_b \equiv 2\gamma - (A_b + 1)$. Recalling that the irrotational energy normalization is given by $(E_m^2)_i = wL/H$, Eq. (106) can be put in the form $\alpha_{1\text{–}4} = \frac{1}{2} K_i M_b$; the irrotational growth rate coefficient is simply

$$K_i = -\gamma_b - \tfrac{4}{3}\xi M_b^2 - \left[1 + M_b^2 \xi^2 l^2 / (m^2 \pi^2)\right]^{-1} \tag{107}$$

The sign of K_i will directly prescribe motor stability. Understanding how K_i changes sign as ξ is varied is the key to studying the changes in the stability behavior. This can be best accomplished by examining Cardano's discriminant for $K_i = 0$. One finds

$$\Delta_i = 9l^2(1+\gamma_b)\gamma_b^3 + m^2\pi^2[27+16\gamma_b(9+4\gamma_b)]M_b^2 \quad (108)$$

When $\Delta_i < 0$, K_i will change sign at the critical damping parameter of

$$\xi_i = \frac{1}{2M_b^2}\left\{\left[\sqrt{\gamma_b^2 - \tfrac{16}{3}m^2\pi^2M_b^2l^{-2}}\,\sin\left(\tfrac{1}{3}\sin^{-1}\left\{\left(\gamma_b^2 - \tfrac{16}{3}m^2\pi^2M_b^2l^{-2}\right)^{-\frac{3}{2}}\left[\gamma_b^3 + (24-16\gamma_b)m^2\pi^2M_b^2l^{-2}\right]\right\}\right) - \tfrac{1}{2}\gamma_b\right]\right\} \quad (109)$$

It may be instructive to note that whenever $\gamma_b < -1$, K_i will be negative, hence indicating a stable system. Conversely, having $\gamma_b > 0$, $K_i > 0$ leads to an unstable case. However, when $\Delta_i < 0$, an unstable system is realized for $\xi > \xi_i$; it appears that the irrotational formulation considered here is missing a key component so long as it predicts a more unstable system with successive increases in friction, or ξ. Physically, increasing ξ at a given oscillation mode number (beyond some critical value) should have a stabilizing effect because it can only be accomplished by increasing the dimensionless viscosity δ, decreasing the surface Mach number, or decreasing the length of the motor. Any of these changes should lead to a more stable system.

Another way of assessing the stability of the system is by examining the other critical values of remaining parameters which may cause the system to cross from stability to instability and vice versa. After some algebra, one finds

$$M_b^* = (8\xi^2l^2)^{-\frac{1}{2}}\left[-3\gamma_b\xi l^2 - 4m^2\pi^2 + \left(9\gamma_b^2\xi^2l^4 + 16m^4\pi^4 - 24\gamma_b\xi l^2m^2\pi^2 - 48\xi\pi^2m^2l^2\right)^{\frac{1}{2}}\right]^{\frac{1}{2}} \quad (110)$$

to be the critical value of the injection Mach number. Moreover one can proceed to find

$$l^* = \left[-\left(\gamma_b + \tfrac{4}{3}\xi M_b^2 + 1\right)\left(\gamma_b + \tfrac{4}{3}\xi M_b^2\right)^{-1}m^2\pi^2\xi^{-2}M_b^{-2}\right]^{\frac{1}{2}} \quad (111)$$

to be the critical characteristic length of the slab motor that will cause a change in the stability status of a given system. As such it can be determined that whenever $M_b < M_b^*$, or $l > l^*$ the system becomes unstable. Note that l^* is unphysical, being purely imaginary.

B. Improved Linear Formulation

For a more precise stability estimation, one must involve all available rotational interactions. This can be accomplished by taking

$$\alpha_r = \alpha_{1\text{–}10} = \sum_{n=1}^{10}\alpha_n \quad (112)$$

where the corrected energy normalization is based on work presented by Flandro and Majdalani [44]

$$\left(E_m^2\right)_r = \tfrac{5}{4}wL/H \quad (113)$$

The superposition of these terms gives $\alpha_{1\text{–}10} = \frac{2}{5}M_bK_r$; the rotational stability coefficient is realizable from

$$K_r = C - \tfrac{4}{3}M_b^2\xi - \tfrac{1}{8}\pi^2M_b^2\left(\xi^2M_b^2 - m^2\pi^2l^{-2}\right)\left(\xi^2M_b^2 + m^2\pi^2l^{-2}\right)^{-2} \quad (114)$$

where

$$C = -\gamma_b + \tfrac{1}{2}\left\{1 - \tfrac{1}{24}\left[m\pi^2\xi^4e^{2\xi}(\pi^2-12)\right]^{-1}\left[\tfrac{39}{85} + \tfrac{1}{82}\xi + \tfrac{7}{13}\exp\left(-\tfrac{107}{50}\xi\right)\right](4m\pi^2+3)[(1+2\xi-e^{2\xi}) + \pi^2\{3e^{2\xi} - 3 - 2\xi[3+\xi(3+2\xi)]\}12\xi^2]\right\} - \tfrac{1}{4}(m\pi\xi)^{-1}(24m-\pi^2)^{-1}\left[\tfrac{21}{32} + \tfrac{19}{56}\exp(-\tfrac{27}{10^5}\xi)\right] \times \left(m\pi - \tfrac{11}{91}\right)(3\xi^{-1}e^{-2\xi}\{16m\xi^2(e^{2\xi}-1) + \pi^2[1 - e^{2\xi} + 2\xi(1+\xi)]\}) \quad (115)$$

Equation (114) enables us to seek direct relations between chamber parameters that will promote a stable system by ensuring a negative K_r. Similar relations can be helpful in the developmental stages of motors exhibiting less simplistic grain configurations.

It is worth mentioning at this point that this expression is valid only when $M_b \le 0.01$ and $\xi \le 1.0$. These ranges encapsulate the parametric spectrum associated with most solid rocket motors.

The complexity of Eq. (115) makes obtaining an analytical expression for the critical value of ξ infeasible. At this point we will only present the critical values of the other key parameters. One finds

$$M_b^* = \frac{m\pi}{\xi l}\{(-\pi^2 + 8C\xi^2)^{-1}[-\tfrac{1}{2}\pi^2 - 8C\xi^2 + \tfrac{1}{2}\pi(\pi^2 + 64C\xi^2)^{\frac{1}{2}}]\}^{\frac{1}{2}} \quad (116)$$

to be the critical value of the injection Mach number. Moreover, one evaluates the critical value of the slab-motor length to be

$$l^* = \frac{m\pi}{\xi M_b}\{(-\pi^2 + 8C\xi^2)^{-1}[-\tfrac{1}{2}\pi^2 - 8C\xi^2 + \tfrac{1}{2}\pi(\pi^2 + 64C\xi^2)^{\frac{1}{2}}]\}^{\frac{1}{2}} \quad (117)$$

In conformance with physical observations, we find that an unstable case follows from $M_b > M_b^*$ or $l > l^*$.

C. Comparing Numerics and Asymptotics

Summarized in Tables 1 and 2 are the results from the irrotational and rotational formulations. These dimensional growth rates are related to the nondimensional values via $\alpha^* = \alpha a_0/H$. In Table 1, all factors are computed by numerically evaluating the volumetric integrals. In Table 2, the analytical expressions derived earlier are used to estimate the corresponding factors. From these tables, one realizes that a significant discrepancy exists between the irrotational prediction $\alpha_{1\text{–}4}^*$ and the rotationally adjusted value $\alpha_{1\text{–}10}^*$. This discrepancy varies from 36% for the equivalent Cold-Flow Experiment to about 111% for the equivalent (slab-scaled) Small Rocket Motor. Again, the latter discrepancy suggests a less stable system than projected by irrotational theory. Clearly, the additional rotational corrections play an essential role in the proper assessment of instability.

Comparing numerical results from Table 1 to analytical ones from Table 2, one can discern the excellent capability of analytical approximations to reproduce the numerically integrated growth rate

Table 1 Numerical integrals of cumulative and individual growth rates ($\sec^{-1}$)

Motor	$\alpha_{1\text{–}4}^*$ [a]	$\alpha_{1\text{–}10}^*$	$\lvert\frac{\Delta\alpha}{\alpha}\rvert$%	α_1^*	α_2^*	α_4^*	α_5^*	α_6^*	α_7^*	α_8^*	α_9^*	α_{10}^*
Small motor	−0.135	39.77	100	36.0	-16.2^{-5}	−36.2	36.2	17.6	−13.8	833^{-5}	1.82	−1.82
Tactical rocket	−27.9	−2.04	92.7	−7.11	-1.43^{-5}	−17.7	17.7	5.95	−0.888	845^{-5}	4.31	−4.31
Cold flow	−38.9	−25.06	35.6	−27.1	-9.54^{-6}	−7.45	7.45	2.56	−0.509	0.0117	1.73	−1.73
Space shuttle SRB	−3.24	−0.50	84.4	−1.08	-4.43^{-8}	−1.80	1.80	0.580	−0.0054	0.0030	0.502	−0.502

[a]The sum of the growth rates is multiplied by $\frac{4}{5}$ to be consistent with the rotational formulation based on an energy normalization value of $(E_m^2)_r = \frac{5}{4}wl$ instead of $(E_m^2)_i = wl$.

Table 2 Analytical estimates of cumulative and individual growth rates ($\sec^{-1}$)

Motor	α^*_{1-4} [a]	α^*_{1-10}	$\lvert\frac{\Delta\alpha}{\alpha}\rvert\%$	α^*_1	α^*_2	α^*_4	α^*_5	α^*_6	α^*_7	α^*_8	α^*_9	α^*_{10}
Small motor	−4.39	39.50	111	36.0	-16.2^{-5}	−39.96	39.96	17.5	−13.95	832^{-5}	1.82	−1.82
Tactical rocket	−28.0	−2.02	92.8	−7.11	-1.43^{-5}	−17.82	17.82	5.96	−0.878	845^{-5}	4.31	−4.31
Cold flow	−39.0	−25.04	35.8	−27.1	-9.54^{-6}	−7.24	7.24	2.57	−0.502	0.0117	1.73	−1.73
Space shuttle SRB	−3.25	−0.50	84.5	−1.08	-4.43^{-8}	−1.81	1.81	0.579	−0.005	0.0030	0.504	−0.504

[a]The sum of the growth rates is multiplied by $\frac{4}{5}$ to be consistent with the rotational formulation based on an energy normalization value of $(E^2_m)_r = \frac{5}{4}wl$ instead of $(E^2_m)_i = wl$.

factors. The encountered error varies from 0% in the equivalent reusable solid rocket motor configuration, to about 1.32% in the equivalent tactical rocket. Because of their asymptotic nature, the analytical expressions can be substituted for rather costly numerical simulations in the domain where the values of $\xi \leq 1.0$ and $M_b \leq 0.01$. This restriction will ensure that the asymptotic approximations used in perturbing the respective growth rate expressions remain valid. The corresponding physical range is in fact quite appropriate for practical motor chamber conditions.

Tables 1 and 2 can be used to assess the order of magnitude of various growth rates. The largest contributors can be readily identified to be pressure coupling, flow turning, rotational flow, mean vorticity, viscosity, pseudovorticity, and unsteady nozzle corrections. Conversely, the dilatational energy, acoustic mean flow, and pseudoacoustic corrections are either vanishingly or negligibly small. Because of intermediate cancellations, only pressure coupling, mean vorticity and viscosity corrections survive in the overall assessment. These must of course be supplemented by corrections due to particle damping, distributed combustion, and two-phase interactions.

D. Growth Rate Sensitivity

An integral part of assessing the acoustic instability growth in solid rocket motors rests in understanding the role that the various working parameters play in this process. To that end, a number of illustrations presented subsequently in this section will describe the effect of varying the key parameters in a fashion that reproduces different operational settings. A careful analysis of these illustrations will further serve to validate the mathematical model as present results will be shown to follow correct physical predictions.

Figure 2 is devoted to showing the stability predictions based on the irrotational formulation in contrast to those based on the approach presented in this study. In Figs. 2a and 2b, numerical stability growth rates based on the current work are plotted versus the viscous parameter at several injection Mach numbers. It is clear that the plots generally follow the physical predictions corroborated by the asymptotic solutions; for example, one notes that an increase in ξ at constant M_b promotes system stability. Conversely, an increase in M_b at constant ξ is destabilizing.

By comparing Figs. 2a and 2b, one can identify the role of viscous friction to be rather unimportant in short motors (e.g., $L/H = 20$); it becomes more appreciable, however, as the length is increased (in Fig. 2b where $L/H = 50$). This result may be ascribed to the longer residence time and trajectory of particles in longer chambers.

Figure 2c displays numerical stability growth rates based on the irrotational formulation as function of the viscous parameter. Note that the trends associated with the irrotational model contradict those presented earlier. From Fig. 2c one can infer that the system becomes less stable as the viscosity of the fluid is increased. Moreover, a decrease in M_b at constant ξ appears to be destabilizing. Despite their unphysicality, these trends are confirmed by the analytical criteria for the irrotational model, namely, Eqs. (109) and (110). The observed irregularity in predicting acoustic instability in the slab-motor configuration has also been reported by Flandro and Majdalani [27] in a similar study of the full-length cylindrical motor. It may be carefully traced back to the retention of flow turning in the three-dimensional irrotational formulation. This term, albeit essential in a fundamentally acoustical representation, is unnecessary in two or three dimensions.

This important observation is further reinforced by the results given in Fig. 3. An increase in δ at constant injection Mach number and motor length (thus an increase in ξ) is shown to predict a more stable system in Figs. 3a and 3b. The rotational stability framework proves to be consistent with the physically stabilizing nature of friction. This is not the case in Figs. 3c and 3d which depict the numerical stability curves based on the virtually one-dimensional formulation. Using the irrotational model, the system grows sharply unstable as viscosity, a salient stability ingredient, is increased.

E. Comparison to Earlier Work on the Cylindrical Chamber

Additional insight may be gained by briefly comparing the results of the planar and cylindrical configurations. To start, we recall from Majdalani and Van Moorhem [17] that an increase in chamber radius results in an increase in the depth of penetration of steady rotational effects. A similar trend characterizes the unsteady rotational effects (see Sec. 8f in Majdalani and Flandro [45]). These too occupy a larger fraction of the chamber with successive increases in curvature. It is clear that the planar geometry, being of infinite radius, exhibits a much larger depth of penetration than that of an internal burning cylinder. Then, by considering that viscous effects are blown off the wall and relocalized to the core region (situated at the edge of the depth of penetration), they play a weaker role in the planar geometry where the viscous shear layer is thinner in comparison to the cylindrical configuration. Figure 4 illustrates this effect by displaying the influence of ξ, the viscous parameter, on motor stability for the slab and cylindrical chambers. As ξ is increased, the combined growth rate factor for the cylindrical motor decreases much more rapidly than that of the slab motor (also seen in Fig. 2). This can be attributed to the larger sensitivity on ξ in the cylindrical case. A

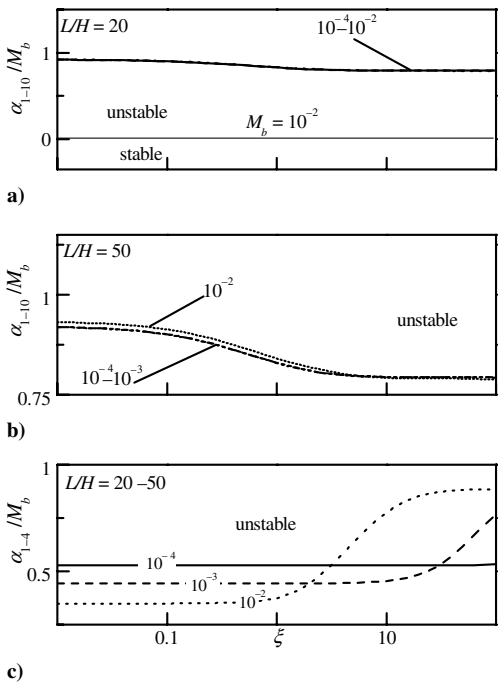

Fig. 2 Numerical stability curves at constant M_b shown over a useful range of ξ and select values of L/H. The system is more sensitive to the stabilizing role of ξ at higher L/H and M_b. Here $A_b^{(r)} = 1.75$, $\gamma = 1.3$, and $m = 1$.

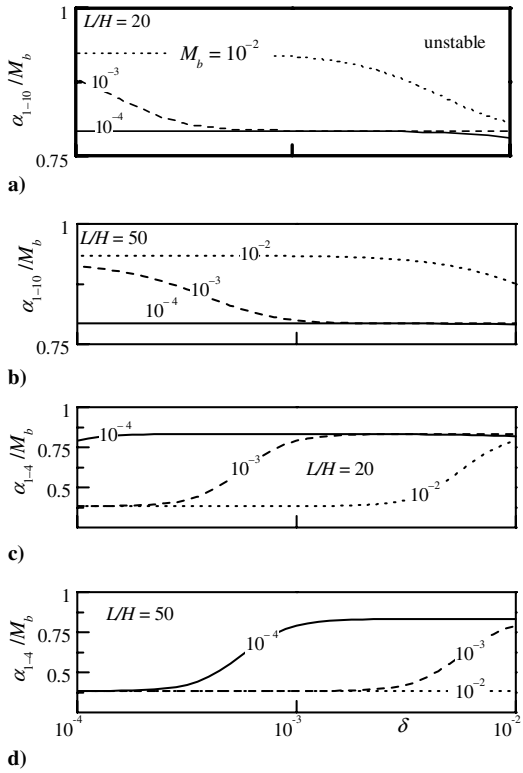

Fig. 3 Numerical stability curves at constant M_b shown over a useful range of δ and select values of L/H. The rotational formulation predicts a less stable system when δ is lowered or when L/H or M_b are increased. This explains, in part, the additional instabilities observed in elongated motors. The irrotational formulation predicts the opposite trends. Here $\gamma = 1.3$ and $m = 1$.

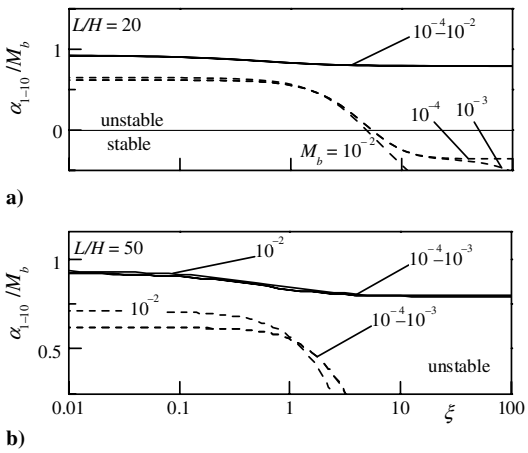

Fig. 4 Numerical stability curves for the slab (solid lines) and cylinder (broken lines) at constant M_b; results are shown over a useful range of ξ and select values of L/H. The system is more sensitive to the stabilizing role of ξ when the curvature is reduced (cylinder) or the Mach number is increased. Here $A_b^{(r)} = 1.75$, $\gamma = 1.3$, and $m = 1$.

similar correlation can be obtained for the combined growth rate and δ. As a final comment, one may note that the equations associated with the planar growth rates are not simpler but rather much more involved than in the cylindrical case. Their evaluation requires the retention of more terms in the integral expansions to yield meaningful results. The stability calculations constitute one of the few cases where the simplicity of the calculations favors the cylindrical geometry.

V. Concluding Remarks

By incorporating the total kinetic energy of the unsteady rotational disturbances into the energy density equation, a more inclusive and physically meaningful assessment of acoustic instability factors has been demonstrated here for the slab rocket motor. The new framework is shown to offer critical advantages which can be used to enhance the widely adopted formulation based on an irrotational representation of the acoustic field. The new formulation gives rise to six additional growth rate terms that have been discounted in irrotational stability models. These include corrections owing to the rotational flow, mean vorticity, viscosity, pseudoacoustic, pseudovorticity, and unsteady nozzle effects. These are summarized in Table 3 in both general and asymptotic forms, including the original corrections evolving from one-dimensional wave theory. The new terms are precipitated, no doubt, from the unsteady rotational disturbances and their interactions with the acoustic wave motion. Interestingly, the rotational flow and unsteady nozzle corrections are identically equal but opposite in sign to the flow turning and pseudovorticity corrections, respectively. At the outset, three linear growth rates survive the attendant cancellations. These are pressure coupling, mean vorticity, and viscosity corrections. Work is under way to incorporate the last two in the standard stability prediction (SSP) code by French, Flandro and Majdalani [46]. This code, which is based on Culick's comprehensive framework [39], is widely used in the propulsion community.

From a physical standpoint, the cancellation of flow turning by another term is confirmed by the 1982 mathematical proof offered by Van Moorhem [47]. In his well-known analysis, Van Moorhem is able to demonstrate that flow turning, which stems from the need to

Table 3 Asymptotic growth rate corrections for the slab motor

	Improved rotational set in general form	Evaluated growth rates (dimensionless)
	$E_m^2 = \frac{1}{2}\iint[(\hat{p}_m)^2 + \hat{\boldsymbol{u}}_m \cdot \hat{\boldsymbol{u}}_m + 2\hat{\boldsymbol{u}}_m \cdot \tilde{\boldsymbol{u}}_m^i + \tilde{\boldsymbol{u}}_m^r \cdot \tilde{\boldsymbol{u}}_m^r + \tilde{\boldsymbol{u}}_m^i \cdot \tilde{\boldsymbol{u}}_m^i]\,\mathrm{d}V$	
α_1: Pressure coupling	$-E_m^{-2}\exp(-2\alpha_m t)\iint\langle\nabla\cdot[\hat{p}\,\hat{\boldsymbol{u}} + \frac{1}{2}M_b\boldsymbol{U}(\hat{p})^2] + M_b[\hat{\boldsymbol{u}}\cdot\nabla(\boldsymbol{U}\cdot\hat{\boldsymbol{u}})]\rangle\,\mathrm{d}V$	$\frac{2}{5}M_b[A_b^{(r)} + 1 - 2\gamma]$
α_2: Dilatational	$E_m^{-2}\exp(-2\alpha_m t)\iint\langle\frac{4}{3}\delta^2\hat{\boldsymbol{u}}\cdot\nabla(\nabla\cdot\hat{\boldsymbol{u}})\rangle\,\mathrm{d}V$	$-\frac{8}{16}\xi M_b^3 \ll \mathcal{O}(1)$
α_3: Acoustic mean	$E_m^{-2}\exp(-2\alpha_m t)\iint\langle M_b\{\hat{\boldsymbol{u}}\cdot(\hat{\boldsymbol{u}}\times\boldsymbol{\Omega})\}\rangle\,\mathrm{d}V$	0
α_4: Flow turning	$E_m^{-2}\exp(-2\alpha_m t)\iint\langle M_b\hat{\boldsymbol{u}}\cdot(\boldsymbol{U}\times\boldsymbol{\omega})\rangle\,\mathrm{d}V$	$-\frac{2}{5}M_b(1+\pi^{-2}M_b^2\xi^2 l^2 m^{-2})^{-1}$
α_5: Rotational flow	$-E_m^{-2}\exp(-2\alpha_m t)\iint\langle\tilde{\boldsymbol{u}}\cdot\nabla\hat{p}\rangle\,\mathrm{d}V$	$\frac{2}{5}M_b(1+\pi^{-2}M_b^2\xi^2 l^2 m^{-2})^{-1}$
α_6: Mean vorticity	$E_m^{-2}\exp(-2\alpha_m t)\iint\langle M_b\tilde{\boldsymbol{u}}(\boldsymbol{U}\times\boldsymbol{\omega})\rangle\,\mathrm{d}V$	$\frac{1}{5}M_b\{1-\frac{1}{24}[m\pi^2\xi^4 e^{2\xi}(\pi^2-12)]^{-1}[\frac{39}{85}+\frac{1}{82}\xi+\frac{7}{13}\exp(-\frac{107}{50})\xi](4m\pi^2+3)\times(12\xi^2(1+2\xi-e^{2\xi})+\pi^2\{3e^{2\xi}-3-2\xi[3+\xi(3+2\xi)]\})\}$
α_7: Viscosity	$-E_m^{-2}\exp(-2\alpha_m t)\iint\langle\delta^2(\hat{\boldsymbol{u}}+\tilde{\boldsymbol{u}})\cdot(\nabla\times\boldsymbol{\omega})\rangle\,\mathrm{d}V$	$-\frac{1}{10}\pi^2(24m-\pi^2)^{-1}ml^{-2}\delta^2\xi^{-3}M_b^{-2}\left[\frac{21}{32}+\frac{19}{56}\exp(-\frac{27}{10}\xi)\right]\left(m-\frac{11}{91}\right)(3e^{-2\xi}\{16m\xi^2\times(e^{2\xi}-1)+\pi^2[1-e^{2\xi}+2\xi(1+\xi)]\})$
α_8: Pseudo acoustic	$E_m^{-2}\exp(-2\alpha_m t)\iint\langle-\hat{\boldsymbol{u}}\cdot\nabla\tilde{p}\rangle\,\mathrm{d}V$	$\frac{9}{25}M_b^3 l^2/m^2 \ll \mathcal{O}(1)$
α_9: Pseudo vorticity	$-E_m^{-2}\exp(-2\alpha_m t)\iint\langle\tilde{\boldsymbol{u}}\cdot\nabla\tilde{p}\rangle\,\mathrm{d}V$	$\frac{2}{15}M_b\left(1-\frac{3}{2}\pi^{-2}\right)\left(\frac{427}{425}+\frac{917}{374}\xi+\frac{95}{61}\xi^2+\frac{437}{670}\xi^3+\frac{101}{847}\xi^4+\frac{1}{65}\xi^5+\frac{1}{794}\xi^6\right)^{-1}$
α_{10}: Unsteady nozzle	$-E_m^{-2}\exp(-2\alpha_m t)\iint\langle M_b(\hat{\boldsymbol{u}}+\tilde{\boldsymbol{u}})\cdot\nabla(\boldsymbol{U}\cdot\tilde{\boldsymbol{u}})\rangle\,\mathrm{d}V$	$-\frac{2}{15}M_b\left(1-\frac{3}{2}\pi^{-2}\right)\left(\frac{427}{425}+\frac{917}{374}\xi+\frac{95}{61}\xi^2+\frac{437}{670}\xi^3+\frac{101}{847}\xi^4+\frac{1}{65}\xi^5+\frac{1}{794}\xi^6\right)^{-1}$

satisfy fundamental conservation laws in a chamber with sidewall mass addition, is a needed adjustment only if a problem is formulated in one-dimensional space. In multidimensional settings, such as those employed in most recent investigations, flow turning is absent.

The second interesting cancellation is that of pseudovorticity by virtue of the unsteady nozzle damping. This outcome brings the results to a closer agreement with conventional theory; the latter downplays the role of the pseudopressure (or pseudosound) in the overall energy assessment. In our problem, the only remaining term due to the pseudopressure is α_8, which is indeed very small and, hence, negligible.

As usual, using the four representative motor properties to define four case studies, the improvements in prediction capability are quantified and shown to be nonnegligible when compared with the irrotational estimates. The analytical expressions presented here for the slab rocket motor are also shown to provide expeditious approximations for the volume integrals that arise in the stability calculations. Generally, the error in the analytical prediction is shown to differ from the numerical solution by a percent or less.

The analytical expressions lead to explicit relations between the salient flow attributes and stability. This permits calculating critical motor lengths and Mach numbers that must not be exceeded if hoping to mitigate acoustic instabilities. Physically, the proposed formulation confirms experimental findings by projecting a less stable environment in longer motors, at higher surface Mach numbers, and for propellants exhibiting higher surface admittance values. In the same vein, a more stable environment is promoted at higher oscillation mode numbers (which absorb more trigger energy) and at increasing levels of viscous damping. The role of the latter becomes more appreciable in longer motors or at higher Mach numbers. Not surprisingly, both irrotational and rotational relations agree on the role of surface admittance, but seem to be conflicting on other counts. For this reason, our study suggests the important physical need to incorporate all rotational corrections in future stability calculations.

In recent years, the slab-motor geometry has increased in popularity, especially, in academic studies of acoustic instability. Our results are hoped to supplement the existing literature and serve as a benchmark for next generation numerical experiments; additional corrections for the slab motor need to be assessed, and these are hoped to be unraveled in forthcoming investigations. Among instability contributors omitted here are corrections due to time-dependence of the mean pressure, particle damping and multiphase interactions, distributed combustion, parietal vortex shedding, and intrinsic mean flow instabilities that have been recently reported by Lupoglazoff and Vuillot [48,49], and Griffond and Casalis [5,6]. It is speculated that such instabilities may appear even in the absence of protrusions, baffles, inhibitors, or intersegmental gaps. The instability discussed by Griffond and Casalis [5,6] appears to be a property of the mean flow itself and may need to be separately accounted for in the overall energy balance. For each of these factors, additional work lies ahead.

Acknowledgments

This project was sponsored by the National Science Foundation through Grant No. CMS-0353518. The authors are thankful for the supplemental support obtained from Software and Engineering Associates, Incorporated.

References

[1] Brownlee, W. G., "Nonlinear Axial Combustion Instability in Solid Propellant Motors," *AIAA Journal*, Vol. 2, No. 2, 1964, pp. 275–284.

[2] Brownlee, W. G., "An Experimental Investigation of Unstable Combustion in Solid Propellant Rocket Motors," Ph.D. Dissertation, California Institute of Technology, 1959.

[3] Brownlee, W. G., and Marble, F. E., "An Experimental Investigation of Unstable Combustion in Solid Propellant Rocket Motors," *ARS Progress in Astronautics and Rocketry: Solid Propellant Rocket Research*, Vol. 1, edited by M. Summerfield, Academic Press Inc., New York, 1960, pp. 455–494.

[4] Casalis, G., Avalon, G., and Pineau, J.-P., "Spatial Instability of Planar Channel Flow with Fluid Injection Through Porous Walls," *Physics of Fluids*, Vol. 10, No. 10, 1998, pp. 2558–2568.

[5] Griffond, J., and Casalis, G., "On the Nonparallel Stability of the Injection Induced Two-Dimensional Taylor Flow," *Physics of Fluids*, Vol. 13, No. 6, 2001, pp. 1635–1644.

[6] Griffond, J., and Casalis, G., "On the Dependence on the Formulation of Some Nonparallel Stability Approaches Applied to the Taylor Flow," *Physics of Fluids*, Vol. 12, No. 2, 2000, pp. 466–468.

[7] Avalon, G., Casalis, G., and Griffond, J., "Flow Instabilities and Acoustic Resonance of Channels with Wall Injection," AIAA Paper 98-3218, July 1998.

[8] Liou, T. M., Lien, W. Y., and Hwang, P. W., "Large-Eddy Simulations of Turbulent Reacting Flows in a Chamber with Gaseous Ethylene Injecting Through the Porous Wall," *Combustion and Flame*, Vol. 99, No. 3–4, 1994, pp. 591–600.

[9] Liou, T. M., Lien, W. Y., and Hwang, P. W., "Transition Characteristics of Flowfield in a Simulated Solid-Rocket Motor," *Journal of Propulsion and Power*, Vol. 14, No. 3, 1998, pp. 282–289.

[10] Liou, T.-M., and Lien, W.-Y., "Numerical Simulations of Injection-Driven Flows in a Two-Dimensional Nozzleless Solid-Rocket Motor," *Journal of Propulsion and Power*, Vol. 11, No. 4, 1995, pp. 600–606.

[11] Apte, S., and Yang, V., "Unsteady Flow Evolution in a Porous Chamber with Surface Mass Injection. Part 1: Free Oscillation," *AIAA Journal*, Vol. 39, No. 8, 2001, pp. 1577–1586.

[12] Apte, S., and Yang, V., "Unsteady Flow Evolution in a Porous Chamber with Surface Mass Injection. Part 2: Acoustic Excitation," *AIAA Journal*, Vol. 40, No. 2, 2002, pp. 244–253.

[13] Chu, W.-W., Yang, V., and Majdalani, J., "Premixed Flame Response to Acoustic Waves in a Porous-Walled Chamber with Surface Mass Injection," *Combustion and Flame*, Vol. 133, No. 6129, 2003, pp. 359–370.

[14] Barron, J., Majdalani, J., and Van Moorhem, W. K., "A Novel Investigation of the Oscillatory Field over a Transpiring Surface," *Journal of Sound and Vibration*, Vol. 235, No. 2, 2000, pp. 281–297.

[15] Ma, Y., Van Moorhem, W. K., and Shorthill, R. W., "Innovative Method of Investigating the Role of Turbulence in the Velocity Coupling Phenomenon," *Journal of Vibration and Acoustics*, Vol. 112, No. 4, 1990, pp. 550–555.

[16] Ma, Y., Van Moorhem, W. K., and Shorthill, R. W., "Experimental Investigation of Velocity Coupling in Combustion Instability," *Journal of Propulsion and Power*, Vol. 7, No. 5, 1991, pp. 692–699.

[17] Majdalani, J., and Van Moorhem, W. K., "Laminar Cold-Flow Model for the Internal Gas Dynamics of a Slab Rocket Motor," *Journal of Aerospace Science and Technology*, Vol. 5, No. 3, 2001, pp. 193–207.

[18] Majdalani, J., Barron, J., and Van Moorhem, W. K., "Inception of Turbulence in the Stokes Boundary Layer over a Transpiring Wall," *Journal of Fluids Engineering*, Vol. 124, No. 9, 2002, pp. 1–7.

[19] Wasistho, B., Haselbacher, A., Najjar, F. M., Tafti, D., Balachandar, S., and Moser, R. D., "Direct and Large Eddy Simulations of Compressible Wall-Injection Flows in Laminar, Transitional, and Turbulent Regimes," AIAA Paper No. 2002-4344, July 2002.

[20] Vuillot, F., and Lupoglazoff, N., "Combustion and Turbulent Flow Effects in 2-D Unsteady Navier–Stokes Simulations of Oscillatory Rocket Motors," AIAA Paper 96-0884, January 1996.

[21] Vuillot, F., Dupays, J., Lupoglazoff, N., Basset, T., and Daniel, E., "2-D Navier–Stokes Stability Computations for Solid Rocket Motors: Rotational, Combustion and Two-Phase Flow Effects," AIAA Paper No. 97-3326, July 1997.

[22] Lupoglazoff, N., and Vuillot, F., "Numerical Simulation of Vortex Shedding Phenomenon in Two-Dimensional Test Case Solid Rocket Motors," AIAA Paper No. 92-0776, January 1992.

[23] Couton, D., Doan-Kim, S., and Vuillot, F., "Numerical Simulation of Vortex-Shedding Phenomenon in a Channel with Flow Induced through Porous Wall," *International Journal of Heat and Fluid Flow*, Vol. 18, No. 3, 1997, pp. 283–296.

[24] Ugurtas, B., Avalon, G., Lupoglazoff, N., and Vuillot, F., "Numerical Computations of Hydrodynamic Instabilities Inside Channels with Wall Injection," AIAA Paper No. 99-2505, June 1999.

[25] Prévost, M., Vuillot, F., and Traineau, J. C., "Vortex-Shedding Driven Oscillations in Subscale Motors for the Ariane 5 MPS Solid Rocket Motors," AIAA Paper No. 96-3247, July 1996.

[26] Chibli, H. A., Majdalani, J., and Flandro, G. A., "Fundamental Growth Rate Corrections in Rocket Motor Stability Calculations," AIAA Paper No. 2002-3610, July 2002.

[27] Flandro, G. A., and Majdalani, J., "Aeroacoustic Instability in Rockets," *AIAA Journal*, Vol. 41, No. 3, 2003, pp. 485–497.

[28] Flandro, G. A., "Solid Propellant Acoustic Admittance Corrections,"

Journal of Sound and Vibration, Vol. 36, No. 3, 1974, pp. 297–312.
[29] Flandro, G. A., "Approximate Analysis of Nonlinear Instability with Shock Waves," AIAA Paper No. 82-1220, July 1982.
[30] Flandro, G. A., "Energy Balance Analysis of Nonlinear Combustion Instability," *Journal of Propulsion and Power*, Vol. 1, No. 3, 1985, pp. 210–221.
[31] Flandro, G. A., "Effects of Vorticity on Rocket Combustion Stability," *Journal of Propulsion and Power*, Vol. 11, No. 4, 1995, pp. 607–625.
[32] Culick, F. E. C., "Stability of Longitudinal Oscillations with Pressure and Velocity Coupling in a Solid Propellant Rocket," *Combustion Science and Technology*, Vol. 2, No. 4, 1970, pp. 179–201.
[33] Culick, F. E. C., "Acoustic Oscillations in Solid Propellant Rocket Chambers," *Acta Astronautica*, Vol. 12, No. 2, 1966, pp. 113–126.
[34] Culick, F. E. C., "Rotational Axisymmetric Mean Flow and Damping of Acoustic Waves in a Solid Propellant Rocket," *AIAA Journal*, Vol. 4, No. 8, 1966, pp. 1462–1464.
[35] Culick, F. E. C., "The Stability of One-Dimensional Motions in a Rocket Motor," *Combustion Science and Technology*, Vol. 7, No. 4, 1973, pp. 165–175.
[36] Culick, F. E. C., "Stability of Three-Dimensional Motions in a Rocket Motor," *Combustion Science and Technology*, Vol. 10, No. 3, 1974, pp. 109–124.
[37] Culick, F. E. C., "Rotational Axisymmetric Mean Flow and Damping of Acoustic Waves in a Solid Propellant Rocket," *Journal of Propulsion and Power*, Vol. 5, No. 6, 1989, pp. 657–664.
[38] Culick, F. E. C., *Combustion Instabilities in Propulsion Systems*, Vol. 4, American Society of Mechanical Engineers, Noise Control and Acoustics Division, New York, 1989, pp. 33–52.
[39] Culick, F. E. C., and Yang, V., "Prediction of the Stability of Unsteady Motions in Solid Propellant Rocket Motors," *Nonsteady Burning and Combustion Stability of Solid Propellants*, Vol. 143, Progress in Astronautics and Aeronautics, edited by L. De Luca, E. W. Price, and M. Summerfield, AIAA, Washington, DC, 1992, pp. 719–779.
[40] Culick, F. E. C., "Combustion Instabilities in Propulsion Systems," *Unsteady Combustion*, Kluwer Academic Publishers, New York, 1996, pp. 173–241.
[41] Majdalani, J., Flandro, G. A., and Fischbach, S. R., "Some Rotational Corrections to the Acoustic Energy Equation in Injection-Driven Enclosures," *Physics of Fluids*, Vol. 17, No. 7, 2005, pp. 07410201–07410220.
[42] Terrill, R. M., "Laminar Flow in a Uniformly Porous Channel," *The Aeronautical Quarterly*, Vol. 15, 1964, pp. 299–310.
[43] Flandro, G. A., "On Flow Turning," AIAA Paper No. 95-2530, July 1995.
[44] Chibli, H. A., Majdalani, J., and Flandro, G. A., "Improved Energy Normalization Function in Rocket Motor Stability Calculations," AIAA Paper No. 2003-5113, July 2003.
[45] Majdalani, J., and Flandro, G. A., "The Oscillatory Pipe Flow with Arbitrary Wall Injection," *Proceedings of the Royal Society of London A*, Vol. 458, No. 2022, 2002, pp. 1621–1651.
[46] French, J. C., Flandro, G. A., and Majdalani, J., "Improvements to the Linear Standard Stability Prediction Program (SSP)," AIAA Paper No. 2004-4181, July 2004.
[47] Van Moorhem, W. K., "Flow Turning in Solid-Propellant Rocket Combustion Stability Analyses," *AIAA Journal*, Vol. 20, No. 10, 1982, pp. 1420–1425.
[48] Lupoglazoff, N., and Vuillot, F., "Numerical Simulations of Parietal Vortex-Shedding Phenomenon in a Cold-Flow Set-Up," AIAA Paper No. 98-3220, July 1998.
[49] Lupoglazoff, N., and Vuillot, F., "Parietal Vortex Shedding as a Cause of Instability for Long Solid Propellant Motors: Numerical Simulations and Comparisons with Firing Tests," AIAA Paper No. 96-0761, January 1996.

J. Oefelein
Associate Editor